batteries

Article

Off-Resonant Dicke Quantum Battery: Charging by Virtual Photons

Giulia Gemme [1], Gian Marcello Andolina [2], Francesco Maria Dimitri Pellegrino [3,4,5], Maura Sassetti [1,6,*] and Dario Ferraro [1,6]

[1] Dipartimento di Fisica, Università di Genova, Via Dodecaneso 33, 16146 Genova, Italy
[2] JEIP, USR 3573 CNRS, Collège de France, PSL Research University, 11 Place Marcelin Berthelot, F-75321 Paris, France
[3] Dipartimento di Fisica e Astronomia "Ettore Majorana", Università di Catania, Via S. Sofia 64, 95123 Catania, Italy
[4] INFN, Sez. Catania, 95123 Catania, Italy
[5] CNR-IMM, Via S. Sofia 64, 95123 Catania, Italy
[6] CNR-SPIN, Via Dodecaneso 33, 16146 Genova, Italy
* Correspondence: sassetti@fisica.unige.it

Abstract: We investigate a Dicke quantum battery in the dispersive regime, where the photons trapped in a resonant cavity are much more energetic with respect to the two-level systems embedded into it. Under such off-resonant conditions, even an empty cavity can lead to the charging of the quantum battery through a proper modulation of the matter–radiation coupling. This counterintuitive behaviour has its roots in the effective interaction between two-level systems mediated by virtual photons emerging from the fluctuations of the quantum electromagnetic field. In order to properly characterize it, we address relevant figures of merit such as the stored energy, the time required to reach the maximum charging, and the averaged charging power. Moreover, the possibility of efficiently extracting energy in various ranges of parameters is discussed. The scaling of stored energy and power as a function of the number N of two-level systems and for different values of the matter–radiation coupling is also discussed, showing, in the strong coupling regime, performances in line with what is reported for the Dicke quantum battery in the resonant regime.

Keywords: quantum batteries; powerful charging; ergotropy; cavity charger

Citation: Gemme, G.; Andolina, G.M.; Pellegrino, F.M.D.; Sassetti, M.; Ferraro, D. Off-Resonant Dicke Quantum Battery: Charging by Virtual Photons. *Batteries* **2023**, *9*, 197. https://doi.org/10.3390/batteries9040197

Academic Editor: Qiang Sun

Received: 27 February 2023
Revised: 20 March 2023
Accepted: 22 March 2023
Published: 25 March 2023

1. Introduction

Quantum batteries (QBs) [1]—genuinely nonclassical devices capable of storing energy and performing useful work—have been a very active topic of research in recent years [2,3]. In this framework, theoretical studies have demonstrated that entangling operations can consistently accelerate the charging [4], with the Dicke quantum battery (QB) standing out as a particularly promising candidate [5–9]. It is given by a system where the energy of photons trapped into a cavity (acting as the charger) is coherently transferred to a QB composed of N quantum units, namely a collection of identical independent two-level systems (TLSs). This model describes, for example, an ensemble of real or artificial atoms embedded in a Fabry–Perot cavity, namely a resonator consisting of two parallel, highly reflective mirrors placed a certain distance apart [10].

In this system, the energy is initially stored into the cavity and flows toward the TLSs due to a proper modulation of the matter–radiation coupling. In order to favour this energy flow the cavity and the TLSs are usually assumed as resonant, namely characterized by the same typical energy. Once the charging process is complete, the coupling between the two systems is turned off, leaving the TLSs in a charged state whose stability crucially depends on relaxation and dephasing times [11–15]. Depending on the conditions, this kind of dissipation can be detrimental for the QB performances [16] or lead counterintuitively to

a stabilization of the devices [17–19] and is usually caused by environmental noise [20] and thermal effects [21]. This kind of device displays a collective speed-up of the charging process. This fact has attracted a great deal of interest and, very recently, a first step toward the realization of a Dicke QB has been experimentally implemented in an excitonic system made of fluorescent organic molecules dispersed in an inert matrix, where the Dicke superabsorption leads to a collective boost of the charging process [22]. Despite this remarkable achievement, the investigation of this kind of device is still in its infancy, and new theoretical and experimental studies could lead to promising routes toward the exploitation of purely quantum effects in miniaturized devices devoted to energy storage.

With this in mind, we want to investigate the role played by exchange of virtual photons between the TLSs composing the QB. A paradigmatic example of the dynamical effect of virtual photons is the Casimir force, which arises from the quantum fluctuations of the electromagnetic field. It was first theoretically investigated by Hendrik Casimir in 1948 [23] and experimentally proven almost 50 years later [24]. This force is due to the presence of virtual photons in the vacuum and, in the case of a Fabry–Perot cavity, depends on the boundary conditions imposed by the mirrors. In particular, in the case of two parallel, uncharged, and perfect metallic plates, the virtual cavity photons are restricted in their fluctuation modes by the plates themselves. As a result, the plates experience a net attractive force.

Motivated by this, we introduce and characterize a new type of device for energy storage where the charging is mediated by virtual photons. In contrast to the conventional Dicke QB, the cavity in our proposed off-resonant Dicke QB can be also empty and the two systems (charger and QB) are far detuned in energy, preventing any direct energy flow between them. This makes the systems easier to realize with respect to the conventional Dicke QB and allows us to describe it in the so-called dispersive regime [25], typically used in quantum computing for qubit readout [26] and characterized by an effective infinite range interaction among the TLSs of the Lipkin–Meshkov–Glick (LMG) kind [27,28]. Our charging protocol works as follows: initially, both the cavity and the QB are in their ground states and decoupled. The cavity mirrors are then brought close together, leading to a finite matter–radiation coupling. Thus, the virtual, detuned photons excite the TLSs and charge the QB. The mirrors are then moved away, switching off again the matter–radiation coupling, leaving the atoms in an excited state. The use of virtual photons in this process gives the QB a unique quantum behaviour. Remarkably enough, in the strong coupling regime, the performances of these off-resonant Dicke quantum batteries are comparable with the ones of the resonant case.

The article is organized as follows. In Section 2, we consider the dispersive regime of the conventional Dicke QB with dipolar matter–radiation coupling. Under the assumption of highly energetic cavity photons, we derive an effective description of the off-resonant Dicke QB based on an LMG model characterized by an infinite range interaction among the TLSs and showing relevant simplifying conservation laws. The charging protocol based on switching on and off the matter–radiation coupling is also discussed. The main figures of merit, namely the energy stored into the QB, the averaged charging power, and the times required to reach their maxima are discussed in Section 3. The ergotropy, namely the maximum energy that can be extracted by means of either collective or individual unitary operation is also introduced. Section 4 reports the results concerning the time evolution of the above quantities for different values of the matter–radiation coupling and at various numbers N of TLSs. The scaling of their maxima as a function of N is also considered. A universal behaviour of the maximum stored energy is discussed in connection with the quantum phase transition predicted for the underlying effective model in Section 5. Section 6 is devoted to the conclusions, while technical details of the calculations are reported in Appendices A–C

2. Model

Let us start by considering a conventional Dicke QB with a dipole matter–radiation coupling between N identical TLSs and a resonant cavity [5]. It is described by the Hamiltonian (from now on, we will set $\hbar = 1$)

$$\begin{aligned} \hat{H}_{\text{Dicke}} &= \hat{H}_B + \hat{H}_C + \hat{H}_{B-C} && (1) \\ &= \omega_z \hat{S}_z + \omega_c \hat{a}^\dagger \hat{a} + 2\lambda \hat{S}_x \left(\hat{a}^\dagger + \hat{a} \right), && (2) \end{aligned}$$

with $\hat{H}_B$ the Hamiltonian of the QB, $\hat{H}_C$ the one of the cavity, and $\hat{H}_{B-C}$ their coupling. In the above equation, we have introduced the collective pseudospin operator

$$\hat{S}_\alpha = \frac{1}{2} \sum_{i=1}^{N} \hat{\sigma}_\alpha^i, \tag{3}$$

with $\hat{\sigma}_\alpha^i$ ($\alpha = x, y, z$) the conventional Pauli matrices associated with the ith TLS and where $\hat{a}$ ($\hat{a}^\dagger$) is the annihilation (creation) operator for the photons in the cavity. Here, ω_z is the level spacing of each TLS, ω_c is the energy of the photons, and λ is the intensity of the matter–radiation coupling. Notice that this configuration can be effectively engineered in conventional cavity [29] and circuit-quantum electrodynamics [30] setups. In the latter case, the TLSs can be realized by means of superconducting qubits coupled to an LC circuit playing the role of a resonant cavity [26].

According to the analysis carried out in Appendix A, considering the Schrieffer–Wolff transformation [25] up to the second order in λ one obtains the effective Hamiltonian

$$\hat{H}_{\text{eff}} = \omega_z \hat{S}_z + \omega_c \hat{a}^\dagger \hat{a} - \frac{2\lambda^2 \omega_z}{\omega_c^2 - \omega_z^2} \hat{S}_z \left(\hat{a}^\dagger + \hat{a} \right)^2 - \frac{4\lambda^2 \omega_c}{\omega_c^2 - \omega_z^2} \hat{S}_x^2, \tag{4}$$

which is a good approximation of the Dicke Hamiltonian in Equation (2) in the dispersive regime $\lambda \ll |\omega_c - \omega_z|$ [25]. Notice that, in this regime, the possibility of increasing the energy stored into a QB through virtual excitations mediated by a higher excited state has been recently discussed [31].

By further considering the condition of highly energetic photons $\omega_c \gg \omega_z$, one finally obtains [32]

$$\hat{H}'_{\text{eff}} = \omega_z \hat{S}_z + \omega_c \hat{a}^\dagger \hat{a} - \frac{4\lambda^2}{\omega_c} \hat{S}_x^2. \tag{5}$$

Getting rid of the cavity contribution, it is possible to map Equation (5) into

$$\begin{aligned} \hat{H} &= \hat{H}_B + \hat{H}_{\text{int}} && (6) \\ &= \omega_z \hat{S}_z - g \hat{S}_x^2, && (7) \end{aligned}$$

with

$$g = \frac{4\lambda^2}{\omega_c}. \tag{8}$$

Notice that, according to this mapping, only positive values of the parameter g are physically meaningful. Moreover, as shown in Appendix A, even a more exotic two-photon matter–radiation coupling [33,34] leads to an analogous effective Hamiltonian.

The Hamiltonian in Equation (7) is characterized by an effective infinite range interaction between the TLSs of the LMG kind [27,28,35] mediated by virtual photons playing the role of a quantum bus [36]. The possibility to achieve high charging power exploiting the entanglement generated in the presence of long-range interaction has been considered in the literature [37,38]. However, the necessity of global operations in order to reach this goal has been recently underlined [39].

In the following, we will assume a charging protocol addressing a time-dependent version of Equation (7),

$$\hat{H}(t) = \hat{H}_B + f(t)\hat{H}_{\text{int}}\,, \tag{9}$$

where $f(t)$ is a classical external control parameter introduced to turn on and off the effective interaction among the TLSs in Equation (7). This can be ultimately seen as a direct consequence of the modulation of the matter–radiation coupling in the original Dicke model in Equation (2) obtained by bringing the cavity mirrors close together. For the sake of simplicity, we will assume this control function to be stepwise: equal to 1 for $t \in [0, \tau_c]$, with τ_c a given time which will be specified in the following, and zero elsewhere. It is worth noting that smoother charging protocols are expected to lead only to marginal changes in the behaviour discussed in the following [40]. Generally speaking, the possibility to optimize the time evolution of the charging protocol has recently been the subject of intense research for both the Dicke QB [9] and other QB technologies [41,42]. Moreover, we further underline the fact that in contrast to what is usually considered [2,3], and in the same spirit of Refs. [43], here the charger is encoded in the effective interaction among the TLSs composing the QB and not into some external classical or quantum device.

Conserved Quantities

In order to investigate the behaviour of QB, for a fixed number N of TLSs, a full numerical exact diagonalization is needed. In order to consistently simplify this task, some symmetries can be exploited.

First of all, the operator

$$\hat{S}^2 = \hat{S}_x^2 + \hat{S}_y^2 + \hat{S}_z^2 \tag{10}$$

is a conserved quantity, namely $\left[\hat{H}(t), \hat{S}^2\right] = 0$. This allows us to work in the $(N+1) \times (N+1)$ Hilbert space with maximal value $s = N/2$ and to characterize the states of the system in terms of a pseudospin basis $|s, m\rangle$, such that

$$\hat{S}^2|s,m\rangle = s(s+1)|s,m\rangle, \tag{11}$$

$$\hat{S}_z|s,m\rangle = m|s,m\rangle, \tag{12}$$

with $m = -s, -s+1, \ldots, s-1, s$.

Moreover, the spin number parity operator

$$\hat{\Pi} = e^{-i\pi\hat{S}_z} \tag{13}$$

satisfies $\left[\hat{H}, \hat{\Pi}\right] = 0$, leading to a further reduction of the Hilbert space dimension for proper initial conditions of the QB. According to this, in the following we will investigate the charging of the QB starting from the ground state of $\hat{H}_B$

$$|\psi(0)\rangle = |\frac{N}{2}, -\frac{N}{2}\rangle. \tag{14}$$

It is worth noting that according to this parity constraint, the perfect charging of the QB, namely the complete transition to the maximally charged state

$$|\psi_{max}\rangle = |\frac{N}{2}, +\frac{N}{2}\rangle, \tag{15}$$

can only occur for an even number N of TLSs. However, as will be clear in the following, the efficiency of this kind of QB is lower than 100%; therefore, we can investigate equivalently both even and odd numbers of TLSs.

3. Figures of Merit

We now introduce relevant quantities able to characterize the performances of the considered off-resonant Dicke QB (with $\omega_c \gg \omega_z$). In the following, we will focus on the

energy stored into the QB itself, the time required to reach the optimal charging, the energy trapped into the interaction term, the averaged charging power, and the ergotropy, namely the maximum amount of work extractable from a charged QB by using either collective or local unitary operations [1,44].

3.1. Stored Energy and Charging Time

First of all, we consider the energy stored into the QB. At a given time t, it is given by [5]

$$E_B(t) = \langle\psi(t)|\hat{H}_B|\psi(t)\rangle - \langle\psi(0)|\hat{H}_B|\psi(0)\rangle, \tag{16}$$

with $|\psi(t)\rangle$ the quantum state of the systems for $t \leq \tau_c$, evolved according to $\hat{H}(t)$.

The charging time, namely the time t_E at which the quantity in Equation (16) reaches its first maximum E_{max}, will be also investigated in the following. Of particular relevance will be the scaling of both E_{max} and t_E as a function of the number N of TLSs composing the QB for different values of the effective coupling g.

It is worth underlining the fact that the system under investigation is considered as closed. This approximation holds as long as the time evolution induced by the external control $f(t)$ is shorter than the typical time scale associated with relaxation of the TLSs t_r [7,16] and the one characterizing the fluctuations of the number of photons in the cavity t_γ [45]. Such conditions can be typically fulfilled in state-of-the-art circuit quantum electrodynamics devices [46,47].

3.2. Averaged Charging Power

Another relevant figure of merit is the averaged charging power, namely the energy stored in a given time, defined as [4,37]

$$P(t) = \frac{E_B(t)}{t}. \tag{17}$$

In analogy with what was done above, we are interested in the scaling of the maximum charging power P_{max} and of the time t_P required to reach it as a function of N and for various values of the effective coupling g.

3.3. Ergotropy

Here, we introduce the ergotropy, namely the maximum work extractable from a QB [44]. We will focus both on the total ergotropy and the one associated with only one of the TLS composing the QB. On a very general ground at a given time t, for an Hamiltonian $\hat{\mathcal{H}}$ and a time-dependent density matrix $\hat{\rho}(t)$ describing a quantum state at a given time, it is possible to define the quantity

$$\mathcal{E}\left(\rho(t), \hat{\mathcal{H}}\right) = \mathrm{tr}[\hat{\mathcal{H}}\hat{\rho}(t)] - \mathrm{tr}[\hat{\mathcal{H}}\hat{\pi}_\rho(t)]\,, \tag{18}$$

with $\hat{\pi}_\rho(t)$ the passive state associated to $\hat{\rho}(t)$ at a given time. Given the diagonal representation of the density matrix

$$\hat{\rho}(t) = \sum_n r_n(t)|r_n(t)\rangle\langle r_n(t)|, \tag{19}$$

with $r_0(t) \geq r_1(t) \geq \cdots$, the associated passive state is diagonal on the eigenbasis of $\hat{\mathcal{H}}$ ($|\epsilon_n\rangle$) and reads

$$\hat{\pi}_\rho(t) = \sum_n r_n(t)|\epsilon_n\rangle\langle\epsilon_n|, \tag{20}$$

with energy eigenstates ordered in such a way that $\epsilon_0 \leq \epsilon_1 \leq \cdots$. This finally leads to the general definition

$$\mathcal{E}\left(\hat{\rho}(t), \hat{\mathcal{H}}\right) = \sum_{k,n} r_k(t)\epsilon_n\Big(|\langle r_k(t)|\epsilon_n\rangle|^2 - \delta_{k,n}\Big), \tag{21}$$

which can be directly applied to our particular case considering

$$\hat{\rho}(t) = |\psi(t)\rangle\langle\psi(t)| \tag{22}$$

and $\hat{\mathcal{H}} = \hat{H}_B$.

Due to the fact that we are considering only unitary operations acting on a closed system, the ergotropy defined above coincides with the energy stored in the QB [1].

With regard to the ergotropy of a single TLS of the QB in Equation (2), one can proceed as follows. The 2×2 reduced density matrix describing the first TLS at a given instant is indicated by $\hat{\rho}_{B,1}$, while the energy is measured with respect to the Hamiltonian

$$\hat{h}_B^1 = \frac{\omega_z}{2}\hat{\sigma}_z^1. \tag{23}$$

Notice that due to the invariance under TLSs permutations of the Hamiltonian in Equation (7), we can focus on the first TLS without any loss of generality. Thus, the maximum energy that can be extracted from a single battery unit in an N TLSs device is given by

$$\mathcal{E}_1^{(N)}(t) \equiv \mathcal{E}(\hat{\rho}_{B,1}(t), \hat{h}_B^1)\,. \tag{24}$$

Consistent with what is done above, this expression can be further simplified by writing $\hat{\rho}_{B,1}(t)$ in the diagonal basis,

$$\hat{\rho}_{B,1}(t) = r_0(t)|r_0(t)\rangle\langle r_0(t)| + r_1(t)|r_1(t)\rangle\langle r_1(t)|\,, \tag{25}$$

where the eigenvalues are again ordered in such a way that $r_0(t) \geq r_1(t)$. In this case, the ergotropy $\mathcal{E}_1^{(N)}(t)$ reduces to

$$\mathcal{E}_1^{(N)}(t) = \frac{E^{(N)}(t)}{N} - r_1(t)\omega_z\,, \tag{26}$$

where we used the fact that $\mathrm{tr}[\hat{\rho}_{B,1}(t)\hat{h}_1^B] = (E^{(N)}(t)/N)$, with $E^{(N)} = \mathrm{tr}[\hat{H}_B\hat{\rho}(t)]$, due to permutation symmetry. We have evaluated the above expression numerically, and further details about this analysis can be found in [9].

We conclude this section by pointing out that for a fixed number N of TLSs, in general,

$$\mathcal{E}(t) \neq N\mathcal{E}_1^{(N)}(t). \tag{27}$$

This is a consequence of the fact that local unitary operations acting on a unique TLS are not enough to extract all the energy stored into the QB, and nonlocal unitary operations collectively acting on the whole QB are needed in order to also extract the energy trapped in the correlations among the elementary building blocks composing the device [1].

4. Results and Scaling Laws

In the following, we will investigate in detail the behaviour of the previously discussed figures of merit for different values of the coupling g and as a function of the number N of TLSs composing the off-resonant Dicke QB.

4.1. Weak Coupling

Let us start by considering the regime $g \ll \omega_z$. The time evolution of the energy stored in the QB and the averaged charging power are reported in Figure 1.

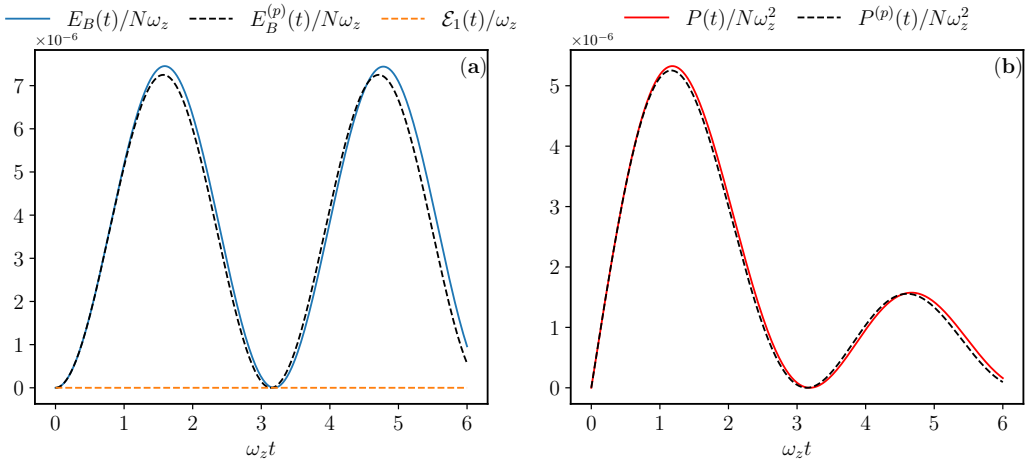

Figure 1. (**a**) Energy stored into the QB $E_B(t)$ (in units of $N\omega_z$) and single TLS ergotropy $\mathcal{E}_1(t)$ (in units of ω_z) as a function of time (in units of ω_z^{-1}) for $N = 30$. (**b**) Averaged charging power $P(t)$ (in units of $N\omega_z^2$) as a function of time (in units of ω_z^{-1}) for $N = 30$. Other parameters are $g = 10^{-3}\omega_z$ and $\omega_z\tau_c > 2\pi$. Black curves represent the theoretical curves obtained through time-dependent perturbative expansions (indicated with the superscript p in the labels) in Equations (28) and (29).

This behavior can be understood considering the analytical expressions for both the above quantities by using a time-dependent perturbative approach (see Appendix B for more details about the derivation). This leads to

$$E_B(t) \approx \frac{g^2}{8}\frac{1-\cos 2\omega_z t}{\omega_z}\Big(N^2 - N\Big) \tag{28}$$

and

$$P(t) \approx \frac{g^2}{8}\frac{1-\cos 2\omega_z t}{\omega_z t}\Big(N^2 - N\Big). \tag{29}$$

These approximated expressions correspond to the black dashed curves reported in Figure 1. For the reported coupling $g = 10^{-3}\omega_z$, they show an excellent agreement with the numerical curves up to $N \approx 30$, further validating the correctness of the considered exact diagonalization and supporting the observation that there is only one relevant frequency of the state dynamics in this regime, leading to very smooth curves with no beats. It is worth noting that the amount of energy stored in this regime is extremely small (see the scale in Figure 1). As a consequence of this, the ergotropy for a single TLS is zero (dashed orange curve in Figure 1); namely, no energy can be extracted for a single TLS by using local unitary operations.

Starting from Equation (28), one can obtain the values of the maximal stored energy and of the charging time associated with the first maximum, namely

$$E_{max} = \frac{g^2}{4\omega_z}\Big(N^2 - N\Big), \tag{30}$$

$$\omega_z t_E = \frac{\pi}{2}, \tag{31}$$

respectively. Analogously, for the averaged charging power in Equation (29) one has

$$P_{max} \approx \frac{g^2}{4.46}\Big(N^2 - N\Big), \tag{32}$$

$$\omega_z t_P \approx 1.16, \tag{33}$$

where the values in this case need to be extracted numerically. The validity of the scalings of stored energy and charging power as a function of the number of TLSs has been checked

in Figure 2. In this framework, we underline the fact that throughout the paper we will consider the scaling at a finite number of TLSs, without addressing the thermodynamical limit, differently from what is discussed for example in [48]. This is justified by the fact that, for example, circuit quantum-electrodynamics devices are usually far from the thermodynamic limit [49].

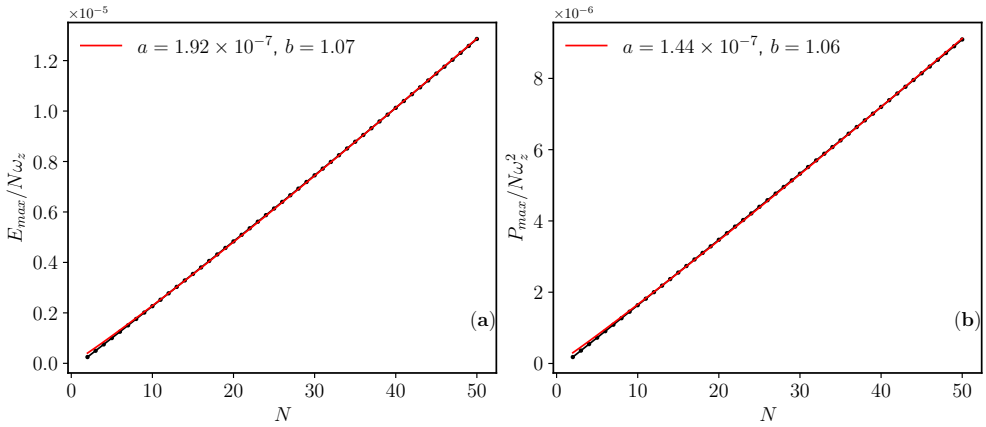

Figure 2. (**a**) Maximum stored energy E_{max} (in units of $N\omega_z$) and (**b**) maximum averaged charging power $P_{\max}$ (in units of $N\omega_z$) as a function of the number of TLSs N (joined black dots). Other parameters are $g = 10^{-3}\omega_z$, $\tau_c = t_E$ in (**a**) and $\tau_c = t_P$ in (**b**). Red curves are the fits of the numerical points according to $E_{max}/N\omega_z = aN^b$ and $P_{max}/N\omega_z^2 = aN^b$. The values of the fitting parameters are indicated in the labels of each panel.

4.2. Strong Coupling

We investigate here the strong coupling regime, namely a situation in which g is of the same order of ω_z [50]. Even if it is difficult to realize in the dissipative Dicke model with dipolar coupling, this situation could be reached by exploiting more exotic matter–radiation couplings, such as the two-photon interaction and properly changing the initial photon distribution in the cavity (see Appendix A for more details). The time evolution of the figures of merits, reported in Figure 3, appears again to be quite regular at small N but shows a complicated beating structure at greater values of N. Notice that, in this regime, the first maximum of the energy stored into the QB is only a local maximum, with higher values of the energy possibly appearing at greater times. However, we focus on it due to the fact that it is characterized by a greater value of the power (see Figure 3d). In this regime, the charging of the QB can exceed 50% near the maxima. In correspondence to these points, one observes the emergence of a nonzero single TLS ergotropy (see the dashed orange curve in Figure 3a,b), the signature of the possibility to extract energy from the QB also by using local unitary operations.

According to the full numerical analysis reported in Figure 4, it is possible to deduce the scaling behaviour of the various figures of merit in the strong coupling regime, namely

$$E_{max} \propto N, \tag{34}$$

$$\omega_z t_E \propto N^{-\frac{1}{2}}, \tag{35}$$

$$P_{max} \propto N^{\frac{3}{2}}, \tag{36}$$

$$\omega_z t_P \propto N^{-\frac{1}{2}}. \tag{37}$$

Notice that these are reminiscent of the ones reported for the Dicke model with conventional dipole matter–radiation coupling [5]. This can be justified by considering the fact that in this case the expectation value of the operator $\hat{S}_x$ over both the ground and the excited states of the system becomes extensively large, similarly to what happens for both $\hat{S}_x$ and the operator $(\hat{a}^\dagger + \hat{a})$ in the original Dicke model in Equation (2) after the superradiant quantum phase transition [51].

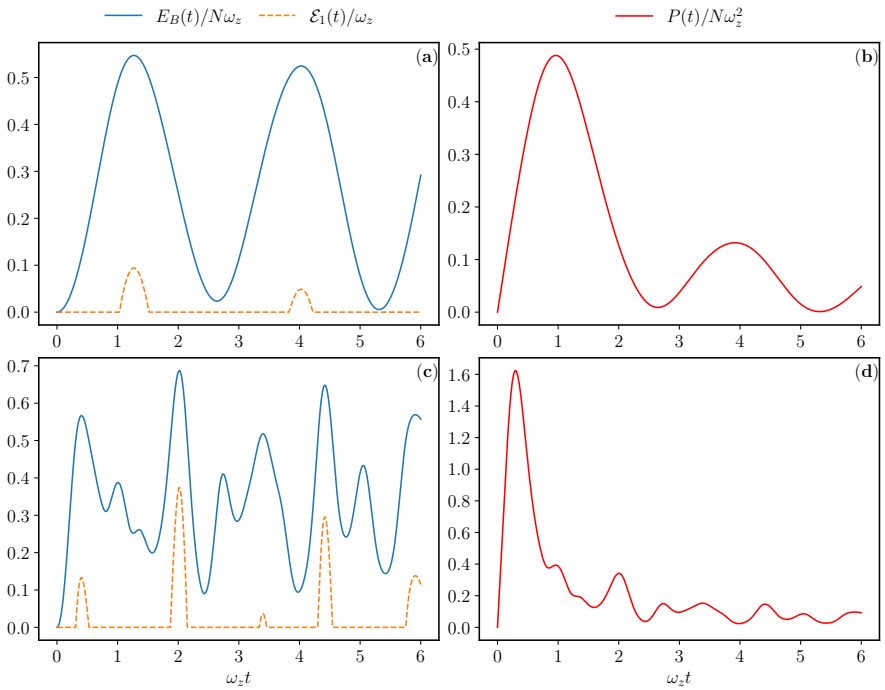

Figure 3. Energy stored into the QB $E_B(t)$ (in units of $N\omega_z$) and single TLS ergotropy $\mathcal{E}_1(t)$ (in units of ω_z) as a function of time (in units of ω_z^{-1}) for $N = 4$ (**a**) and $N = 30$ (**c**). Averaged charging power $P(t)$ (in units of $N\omega_z^2$) and a function of time (in units of ω_z^{-1}) for $N = 4$ (**b**) and $N = 30$ (**d**). Other parameters are $g = \omega_z$ and $\omega_z\tau_c > 2\pi$.

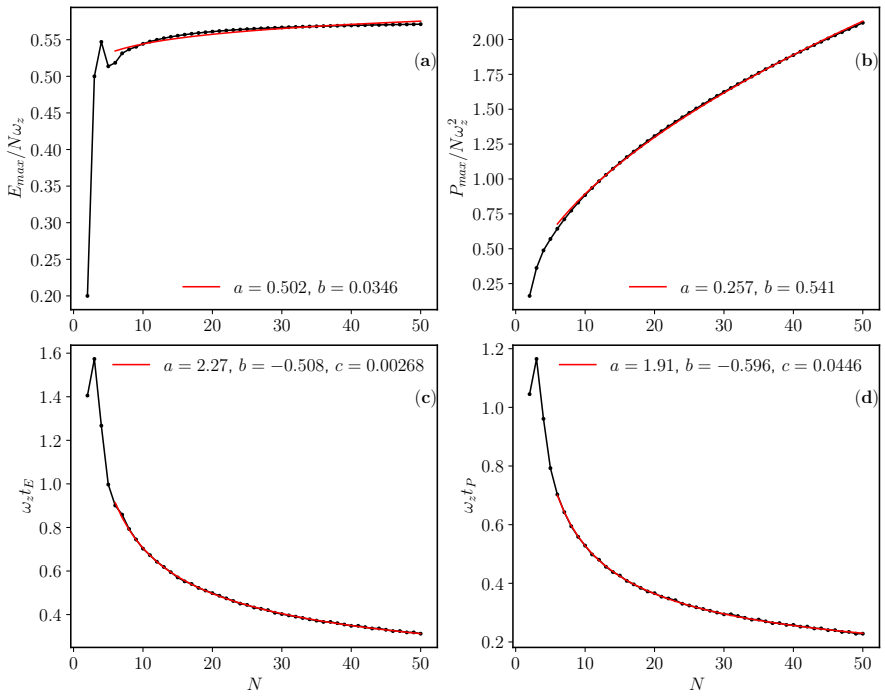

Figure 4. Maximum stored energy E_{max} (in units of $N\omega_z$) (**a**) and corresponding charging time $\omega_z t_E$ (**c**) as a function of the number of TLSs N. Maximum averaged charging power $P_{\max}$ (in units of $N\omega_z^2$) (**b**) and corresponding charging time $\omega_z t_P$ (**d**) as a function of the number of TLSs N (joined black dots). Other parameters are $g = \omega_z$, $\tau_c = t_E$ for each N in (**a**,**c**) and $\tau_c = t_P$ for each N in (**b**,**d**). Red curves are the fits of the numerical points according to $E_{max}/N\omega_z = aN^b$ (**a**), $P_{max}/N\omega_z^2 = aN^b$ (**b**), $\omega_z t_E = aN^b + c$ (**c**), and $\omega_z t_P = aN^b + c$ (**d**). The values of the fitting parameters are indicated in the labels of each panel.

5. Considerations about Universality

The previous analysis showed two drastically different scaling behaviours of the considered quantities for different regimes of the coupling, with the weak coupling showing a better scaling with N and the strong coupling regime more promising in terms of absolute values of the energy storage, charging power, and ergotropy. These are summarized in Table 1. Notice that for intermediate values of the coupling, a crossover between the two behaviour emerges (not shown).

Table 1. Scaling behaviour for some figures of merit in the weak and strong coupling regimes.

Coupling Regime	E_{max}	P_{max}	t_E, t_P
Weak coupling	N^2	N^2	Constant
Strong coupling	N	$N^{\frac{3}{2}}$	$N^{-\frac{1}{2}}$

This change of behaviours can be seen as a consequence of the excited state quantum phase transition (ESQPT) shown by both the Dicke and the effective LMG model (see [52] for a review on the subject). This represents the footprint of a quantum phase transition at the level of the excited states of the system. Its role in the present QB is justified by the fact that it is initialized in the ground state and charged by means of a protocol which naturally involves the excited states. In order to better clarify this point, we can consider the evolution of E_{max} as a function of the renormalized coupling $G = gN$ (see Figure 5). The choice of this renormalized parameter to characterize the evolution of the system can be justified by considering the classical limit of the effective LMG model (see Appendix C for more details) and reminiscent of the renormalization $\Lambda = \lambda\sqrt{N}$ observed for the Dicke model [5]. Notice that the emergence of a crossover behaviour for the maximum stored energy is motivated by the fact that it is closely related to the order parameter of the system, namely the total magnetization, which at a given time t that can be written as

$$\mathcal{M}(t) = \langle\psi(t)|\hat{S}_z|\psi(t)\rangle = \frac{E_B(t)}{\omega_z} + \langle\psi(0)|\hat{S}_z|\psi(0)\rangle. \tag{38}$$

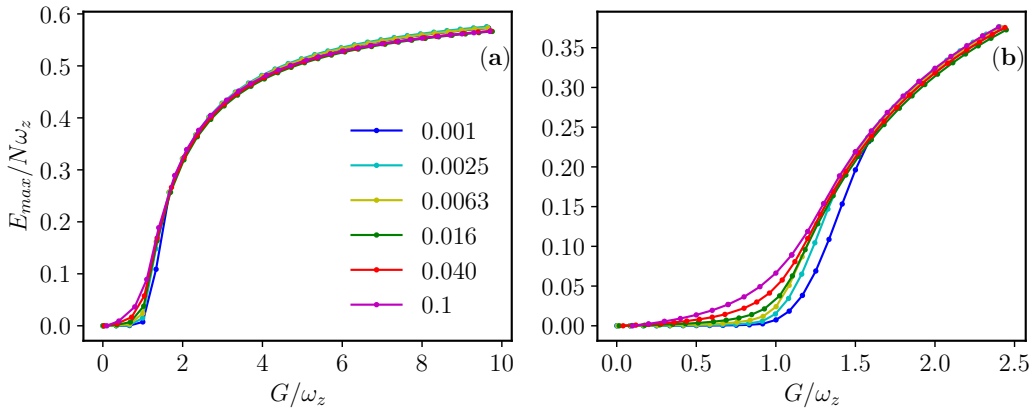

Figure 5. Behaviour of E_{max} (in units of $N\omega_z$) as a function of the rescaled coupling $G = gN$ (in units of ω_z) for various values of g (**a**) and its zoom around the crossover at $G = \omega_z$ (**b**). Values of the coupling are reported in the color scale of the legend, while we have assumed $\tau_c = t_E$ for each value of N.

It is possible to observe now two different regimes for $G < \omega_z$ and $G > \omega_z$, respectively, with a crossover in correspondence of the ESQPT of the model, occurring at $G = \omega_z$. Incidentally, by increasing the value of G (Figure 5b) one finds that the maximum value of energy per TLS reachable in the considered QB can exceed 60%. Remarkably enough, this value is compatible with what is observed for the Dicke model in the strong coupling regime and under resonant conditions [5]. This makes the present off-resonant Dicke QB

competitive for practical experimental realizations, also taking into account the fact that it can be realized by also using a vacuum cavity, which is easier to be engineered and more stable with respect to what happens in the resonant Dicke QB. Moreover, the dependence on the renormalized coupling G allows one to extend the validity of the previous analysis carried out for the strong coupling regime by increasing the number of TLS composing the QB.

6. Conclusions

We have investigated an off-resonant Dicke QB, namely a device composed by N TLSs embedded into a highly detuned resonant cavity. Under this condition, the TLSs feel an effective infinite range interaction among them. By properly switching on and off this coupling, it is possible to promote at least a part of the TLSs from the ground to the excited states, thus charging the QB, even in the case of an empty cavity. This phenomenology can be ultimately related to the exchange of virtual photons whose coupling with the TLSs is varied, bringing the mirrors of the cavity close together.

By looking at relevant figures of merits such as the stored energy, the averaged charging power, and the time required to reach their respective maxima, we have characterized the performance of this kind of system. We have identified a small coupling regime, showing a very poor charging and no possibility of energy extraction (single TLS ergotropy) despite the relevant scaling in both the energy and the averaged charging power, and a strong coupling limit showing the same collective advantage in averaged charging power of the conventional Dicke QB [5] with dipole matter–radiation interaction and in resonant conditions. The crossover between these two regimes is related to the quantum phase transition occurring in the effective model describing the QB [52].

The present device shows, above the critical coupling, performances comparable to the ones of the Dicke QB in the resonant regime. In addition, the observed physics can be obtained by also working with an empty cavity, thus avoiding the need of controlling the initial quantum state of radiation, the physically relevant parameters of the system, or exotic matter–radiation interactions [6]. These remarkable properties make it a very convincing candidate for future practical implementations of a functioning QB in various platforms already considered in the framework of the Dicke QB, such as superconducting qubits or array of semiconducting quantum dots coupled to an LC circuit through a tunable capacitance [53,54].

Author Contributions: Conceptualization, G.M.A. and D.F.; methodology, G.M.A. and D.F.; software, G.G. and G.M.A.; validation, F.M.D.P. and G.M.A.; formal analysis, D.F.; investigation, G.M.A. and G.G.; data curation, G.G.; writing—original draft preparation, D.F. and G.G.; writing—review and editing, G.M.A., F.M.D.P. and M.S.; supervision, M.S. All authors have read and agreed to the published version of the manuscript.

Funding: D.F. would like to thank the funding of the European Union-NextGenerationEU through the "Quantum Busses for Coherent Energy Transfer" (QUBERT) project, in the framework of Curiosity Driven 2021 initiative of the University of Genova. F.M.D.P. was supported by the Università degli Studi di Catania, Piano di Incentivi per la Ricerca di Ateneo 2020/2022 (progetto QUAPHENE), and PNRR MUR project PE0000023-NQSTI.

Institutional Review Board Statement: Not applicable.

Informed Consent Statement: Not applicable.

Data Availability Statement: Data are available from the authors upon request.

Acknowledgments: The authors thank A. Crescente, G. Falci, L. Giannelli, and E. Paladino for illuminating discussions and fruitful comments.

Conflicts of Interest: The authors declare no conflict of interest.

Abbreviations

The following abbreviations are used in this manuscript:

QB	Quantum battery
TLS	Two-level system
LMG	Lipkin–Meshkov–Glick
ESQPT	Excited state quantum phase transition

Appendix A. Derivation of the Effective LMG Hamiltonian

Appendix A.1. Basics of the Schrieffer–Wolff Transformation

Given a generic Hamiltonian $\hat{\mathcal{H}}$ and an operator $\hat{\mathcal{S}}$, it is possible to define

$$\hat{\mathcal{H}}' = e^{\hat{\mathcal{S}}} \hat{\mathcal{H}} e^{-\hat{\mathcal{S}}}. \tag{A1}$$

According to the Baker–Campbell–Hausdorff relation, one can develop the exponential operators in such a way that

$$\hat{\mathcal{H}}' = \hat{\mathcal{H}} + [\hat{\mathcal{S}}, \hat{\mathcal{H}}] + \frac{1}{2!}[\hat{\mathcal{S}}, [\hat{\mathcal{S}}, \hat{\mathcal{H}}]] + \ldots. \tag{A2}$$

On a general ground, one can now assume that it is possible to decompose $\hat{\mathcal{H}}$ in a free and an interacting term, namely

$$\hat{\mathcal{H}} = \hat{\mathcal{H}}_0 + \hat{\mathcal{V}}. \tag{A3}$$

By properly choosing the operator $\hat{\mathcal{S}}$ in such a way to satisfy

$$[\hat{\mathcal{H}}_0, \hat{\mathcal{S}}] = \hat{\mathcal{V}}, \tag{A4}$$

one obtains

$$\hat{\mathcal{H}}' = \hat{\mathcal{H}}_0 + \frac{1}{2}[\hat{\mathcal{S}}, \hat{\mathcal{V}}] + \frac{1}{2}[\hat{\mathcal{S}}, [\hat{\mathcal{S}}, \hat{\mathcal{V}}]] + \ldots. \tag{A5}$$

Assuming now that both $\hat{\mathcal{S}}$ and $\hat{\mathcal{V}}$ depend linearly on a given coupling constant, one can consider a second-order expansion, leading to an effective Hamiltonian of the form

$$\hat{\mathcal{H}}_{\text{eff}} = \hat{\mathcal{H}}_0 + \frac{1}{2}[\hat{\mathcal{S}}, \hat{\mathcal{V}}]. \tag{A6}$$

In the following, we will apply this general scheme to the Dicke model assuming both single- and two-photon interaction.

Appendix A.2. Dicke Model with Single-Photon Coupling

In the case of the Dicke model with conventional dipole matter–radiation coupling [10,25] in Equation (2), one can identify (using the notation of the main text)

$$\hat{\mathcal{H}}_0 = \omega_z \hat{S}_z + \omega_c \hat{a}^\dagger \hat{a}, \tag{A7}$$

$$\hat{\mathcal{V}} = 2\lambda \hat{S}_x \left(\hat{a}^\dagger + \hat{a}\right), \tag{A8}$$

and consequently

$$\hat{\mathcal{S}} = \frac{\lambda}{\omega_c - \omega_z}\left[\hat{S}_- \hat{a}^\dagger - \hat{S}_+ \hat{a}\right] + \frac{\lambda}{\omega_c + \omega_z}\left[\hat{S}_+ \hat{a}^\dagger - \hat{S}_- \hat{a}\right], \tag{A9}$$

with

$$\hat{S}_\pm = \hat{S}_x \pm i\hat{S}_y. \tag{A10}$$

Notice that both Equations (A8) and (A9) are linear in the matter–radiation coupling λ as required by the previous discussion. Using the Schrieffer–Wolff transformation discussed above, one obtains the effective Hamiltonian

$$\hat{\mathcal{H}}_{\text{eff}} = \omega_z \hat{S}_z + \omega_c \hat{a}^\dagger \hat{a} - \frac{2\lambda^2 \omega_z}{\omega_c^2 - \omega_z^2} \hat{S}_z \left(\hat{a}^\dagger + \hat{a}\right)^2 - \frac{4\lambda^2 \omega_c}{\omega_c^2 - \omega_z^2} \hat{S}_x^2, \tag{A11}$$

which is a good approximation of the Dicke Hamiltonian in the so-called dispersive regime $\lambda \ll |\omega_c - \omega_z|$ [25]. By further considering the limit $\omega_c \gg \omega_z$, one finally has

$$\hat{\mathcal{H}}'_{\text{eff}} = \omega_z \hat{S}_z + \omega_c \hat{a}^\dagger \hat{a} - \frac{4\lambda^2}{\omega_c} \hat{S}_x^2. \tag{A12}$$

Getting now rid of the cavity contribution, it is possible to map Equation (A12) into Equation (7) by defining

$$g = \frac{4\lambda^2}{\omega_c}. \tag{A13}$$

Appendix A.3. Dicke Model with Two-Photon Coupling

This more exotic interaction can be obtained by properly engineering both atomic and solid state systems [33,34]. Here, one can write the Hamiltonian

$$\hat{H}^{2ph}_{\text{Dicke}} = \omega_z \hat{S}_z + \omega_c \hat{a}^\dagger \hat{a} + 2\lambda \hat{S}_x \left[\left(\hat{a}^\dagger\right)^2 + (\hat{a})^2\right], \tag{A14}$$

identifying

$$\hat{\mathcal{H}}_0 = \omega_z \hat{S}_z + \frac{\omega_c}{2} \hat{a}^\dagger \hat{a}, \tag{A15}$$

$$\hat{\mathcal{V}} = 2\lambda \hat{S}_x \left[\left(\hat{a}^\dagger\right)^2 + \hat{a}^2\right], \tag{A16}$$

and consequently

$$\hat{\mathcal{S}} = \frac{\lambda}{\omega_c - \omega_z} \left[\hat{S}_- \left(\hat{a}^\dagger\right)^2 - \hat{S}_+ \hat{a}^2\right] + \frac{\lambda}{\omega_c + \omega_z} \left[\hat{S}_+ \left(\hat{a}^\dagger\right)^2 - \hat{S}_- \hat{a}^2\right]. \tag{A17}$$

According to the previous analysis, one obtains the effective Hamiltonian

$$\hat{\mathcal{H}}^{2ph}_{\text{eff}} = \omega_z \hat{S}_z + \frac{\omega_c}{2} \hat{a}^\dagger \hat{a} - \frac{2\lambda^2 \omega_z}{\omega_c^2 - \omega_z^2} \hat{S}_z \left[\hat{a}^2 + \left(\hat{a}^\dagger\right)^2\right]^2 - \frac{4\lambda^2 \omega_c}{\omega_c^2 - \omega_z^2} \hat{S}_x^2 \left(\hat{a}\hat{a}^\dagger + \hat{a}^\dagger \hat{a}\right), \tag{A18}$$

which again represents a good approximation of the two-photon Dicke Hamiltonian in the dispersive limit $\lambda \ll |\omega_c - \omega_z|$.

Further considering the limit $\omega_c \gg \omega_z$, one finally has

$$\hat{\mathcal{H}}'^{2ph}_{\text{eff}} = \omega_z \hat{S}_z + \frac{\omega_c}{2} \hat{a}^\dagger \hat{a} - \frac{4\lambda^2}{\omega_c} (2\hat{a}^\dagger \hat{a} + 1) \hat{S}_x^2. \tag{A19}$$

For proper initial states of the photon in the cavity, it is possible to map Equation (A19) into Equation (7) (up to a constant) by defining

$$g = \frac{4\lambda^2}{\omega_c} (2n + 1), \tag{A20}$$

with n the averaged number of photons into the cavity. Notice that in this case the renormalization of the effective coupling due to the presence of the cavity photons can be exploited to increase the value of g with respect to the previous case.

Appendix B. Perturbative Approach to the Weak Coupling Case

It is possible to study the dynamics induced by Equation (7) and the figures of merits discussed in the main text by applying the time-dependent perturbation theory in terms of the Dyson series.

Working in the interaction picture (indicated in the following by the apex I), the time evolution operator $\hat{U}_I(t,0)$ from the initial time $t = 0$ to a generic time t satisfies the differential equation

$$i\partial_t \hat{U}_I(t,0) = \hat{H}^I_{\rm int}(t)\hat{U}_I(t,0), \tag{A21}$$

with

$$\begin{aligned}\hat{H}^I_{\rm int}(t) &= -g e^{i\omega_z t\hat{S}_z}\hat{S}_x^2 e^{-i\omega_z t\hat{S}_z}\\ &= -g e^{i\omega_z t\hat{S}_z}\hat{S}_x e^{-i\omega_z t\hat{S}_z} e^{i\omega_z t\hat{S}_z}\hat{S}_x e^{-i\omega_z t\hat{S}_z}\\ &= -g\Big[\cos(\omega_z t)\hat{S}_x^2 - \sin(\omega_z t)\cos(\omega_z t)\big(\hat{S}_x\hat{S}_y + \hat{S}_y\hat{S}_x\big) + \sin(\omega_z t)\hat{S}_y^2\Big].\end{aligned} \tag{A22}$$

Imposing the initial condition $\hat{U}_I(0,0) = 1$ and formally integrating the above equation, we have

$$\hat{U}_I(t,0) = 1 - i\int_0^t \hat{H}^I_{\rm int}(t')\hat{U}_I(t',0)dt'. \tag{A23}$$

We can solve iteratively this equation in terms of Dyson's series [55]

$$\hat{U}_I(t,0) = 1 - i\int_0^t \hat{H}^I_{\rm int}(t')dt' + (-i)^2\int_0^t dt'\int_0^{t'} dt''\hat{H}^I_{\rm int}(t')\hat{H}^I_{\rm int}(t'') + \ldots. \tag{A24}$$

In this picture, the energy stored in the QB can be written as

$$\begin{aligned}E_B(t) &= \langle\tfrac{N}{2},-\tfrac{N}{2}|e^{-i\hat{H}_0 t}\hat{U}_I^\dagger(t,0)\hat{H}_B\hat{U}_I(t,0)e^{i\hat{H}_0 t}|\tfrac{N}{2},-\tfrac{N}{2}\rangle\\ &- \langle\tfrac{N}{2},-\tfrac{N}{2}|\hat{H}_B|\tfrac{N}{2},-\tfrac{N}{2}\rangle\\ &= \langle\tfrac{N}{2},-\tfrac{N}{2}|\hat{U}_I^\dagger(t,0)\hat{H}_B\hat{U}_I(t,0)|\tfrac{N}{2},-\tfrac{N}{2}\rangle + \tfrac{\omega_z}{2}N.\end{aligned} \tag{A25}$$

After some long and tedious algebra, one finally obtains

$$E_B(t) = \frac{g^2}{8}\frac{1-\cos 2\omega_z t}{\omega_z}\Big(N^2 - N\Big), \tag{A26}$$

and consequently

$$P(t) = \frac{E(t)}{t} = \frac{g^2}{8}\frac{1-\cos 2\omega_z t}{t\omega_z}\Big(N^2 - N\Big). \tag{A27}$$

Appendix C. Comments on the Classical Limit

In the main text, we have considered the scaling at a finite number of TLSs, without addressing the thermodynamical limit needed for a proper study of the ESQPT. Some hints in this direction can be derived starting from the classical version of the Hamiltonian in Equation (7). This can be obtained by replacing the operators $\hat{S}_{x,y,z}$ with the classical angular momentum components

$$S_x = \frac{N}{2}\sin\theta\cos\varphi, \tag{A28}$$

$$S_y = \frac{N}{2}\sin\theta\sin\varphi, \tag{A29}$$

$$S_z = \frac{N}{2}\cos\theta. \tag{A30}$$

This leads to the classical Hamiltonian

$$H_{\rm cl} = \omega_z \frac{N}{2} \cos\theta - g\frac{N^2}{4} \sin^2\theta \cos^2\varphi. \tag{A31}$$

One can identify now two conjugated variables [56]

$$q = N\cos\theta, \tag{A32}$$

$$p = \varphi, \tag{A33}$$

in such a way that

$$H_{\rm cl} = \frac{\omega_z}{2} q - \frac{g}{4} N^2 \cos^2 p + \frac{g}{4} q^2 \cos^2 p. \tag{A34}$$

Recalling the equations of motion

$$\frac{dq}{dt} = \frac{\partial H_{\rm cl}}{\partial p} = \frac{g}{4} N^2 \sin 2p - \frac{g}{4} q^2 \sin 2p, \tag{A35}$$

$$\frac{dp}{dt} = -\frac{\partial H_{\rm cl}}{\partial q} = -\frac{\omega_z}{2} + \frac{g}{2} q \cos^2 p. \tag{A36}$$

Further manipulating the above equations introducing rescaled and shifted variables

$$q = N\tilde{q}, \tag{A37}$$

$$p = \tilde{p} - \frac{\omega_z}{2} t, \tag{A38}$$

one has

$$\frac{d\tilde{q}}{dt} = \frac{g}{4} N(1-\tilde{q}^2) \sin(2\tilde{p} - \omega_z t), \tag{A39}$$

$$\frac{d\tilde{p}}{dt} = -\frac{g}{2} N\tilde{q} \cos^2\left(\tilde{p} - \frac{\omega_z}{2} t\right), \tag{A40}$$

where the dependence on the renormalized interaction parameter

$$G = gN \tag{A41}$$

emerges, which plays a major role in the discussion about the universality reported in the main text.

References

1. Alicki, R.; Fannes, M. Entanglement boost for extractable work from ensembles of quantum batteries. *Phys. Rev. E* **2013**, *87*, 042123. [CrossRef]
2. Campaioli, F.; Pollock, F.A.; Vinjanampathy, S. *Thermodynamics in the Quantum Regime*; Springer Nature Switzerland AG: Cham, Switzerland, 2018.
3. Bhattacharjee, S.; Dutta, A. Quantum thermal machines and batteries. *Eur. Phys. J. B* **2021**, *94*, 239. [CrossRef]
4. Binder, F.C.; Vinjanampathy, S.; Modi, K.; Goold, J. Quantacell: Powerful charging of quantum batteries. *New J. Phys.* **2015**, *17*, 075015. [CrossRef]
5. Ferraro, D.; Campisi, M.; Andolina, G.M.; Pellegrini, V.; Polini, M. High-Power Collective Charging of a Solid-State Quantum Battery. *Phys. Rev. Lett.* **2018**, *120*, 117702. [CrossRef] [PubMed]
6. Crescente, A.; Carrega, M.; Sassetti, M.; Ferraro, D. Ultrafast charging in a two-photon Dicke quantum battery. *Phys. Rev. B* **2020**, *102*, 245407. [CrossRef]
7. Dou, F.-Q.; Lu, Y.-Q.; Wang, Y.-J.; Sun, J.-A. Extended Dicke quantum battery with interatomic interactions and driving field. *Phys. Rev. B* **2022**, *105*, 115405. [CrossRef]
8. Dou, F.-Q.; Yang, F.-M. Superconducting transmon qubit-resonator quantum battery. *Phys. Rev. A* **2023**, *107*, 023725. [CrossRef]
9. Erdman, P.A.; Andolina, G.M.; Giovannetti, V.; Noé, F. Reinforcement learning optimization of the charging of a Dicke quantum battery. *arXiv* **2022**, arXiv:2212.12397v1.
10. Dicke, H.R. Coherence in Spontaneous Radiation Processes. *Phys. Rev.* **1954**, *93*, 99. [CrossRef]

11. Santos, A.C.; Cakmak, B.; Campbell, S.; Zinner, N.T. Stable adiabatic quantum batteries. *Phys. Rev. E* **2019**, *100*, 032107. [CrossRef]
12. Barra, F. Dissipative Charging of a Quantum Battery. *Phys. Rev. Lett.* **2019**, *122*, 210601. [CrossRef] [PubMed]
13. Zakavati, S.; Tabesh, F.T.; Salimi, S. Bounds on charging power of open quantum batteries. *Phys. Rev. E* **2021** *104*, 054117. [CrossRef]
14. Morrone, D.; Rossi, M.A.C.; Smirne, A.; Genoni, M.G. Charging a quantum battery in a non-Markovian environment: A collisional model approach. *arXiv* **2022**, arXiv:2212.13488v1.
15. Gemme, G.; Grossi, M.; Ferraro, D.; Vallecorsa, S.; Sassetti, M. IBM Quantum Platforms: A Quantum Battery Perspective. *Batteries* **2022**, *8*, 43. [CrossRef]
16. Carrega, M.; Crescente, A.; Ferraro, D.; Sassetti, M. Dissipative dynamics of an open quantum battery. *New J. Phys.* **2020**, *22*, 083085. [CrossRef]
17. Quach, J.Q.; Munro, W.J. Using Dark States to Charge and Stabilize Open Quantum Batteries. *Phys. Rev. Appl.* **2020** *14*, 024092. [CrossRef]
18. Bai, S.-Y.; An J.-H. Floquet engineering to reactivate a dissipative quantum battery. *Phys. Rev. A* **2020** *102*, 060201(R). [CrossRef]
19. Ghosh, S.; Chanda, T.; Mal, S.; Sen(De), A. Fast charging of a quantum battery assisted by noise. *Phys. Rev. A* **2021** *104*, 032207. [CrossRef]
20. Zhao, F.; Dou, F.-Q.; Zhao, Q. Quantum battery of interacting spins with environmental noise. *Phys. Rev. A* **2021** *103*, 033715. [CrossRef]
21. Dağ, C.B.; Niedenzu, W.; Ozaydin, F.; Müstecaplioğlu, Ö.E.; Kurizk, G. Temperature Control in Dissipative Cavities by Entangled Dimers. *J. Phys. Chem. C* **2019**, *123*, 4035–4043 [CrossRef]
22. Quach, J.Q.; McGhee, K.E.; Ganzer, L.; Rouse, D.M.; Lovett, B.W.; Gauger, E.M.; Keeling, J.; Cerullo, G.; Lidzey, D.G.; Virgili, T. Superabsorption in an organic microcavity: Toward a quantum battery. *Sci. Adv.* **2022**, *8*, eabk3160. [CrossRef]
23. Casimir, H.B.G.; Polder, D. The Influence of Retardation on the London-van der Waals Forces. *Phys. Rev.* **1948**, *73*, 360. [CrossRef]
24. Lamoreaux, S.K. Demonstration of the Casimir Force in the 0.6 to 6 μm Range. *Phys. Rev. Lett.* **1997**, *78*, 5. [CrossRef]
25. Schleich, W.P. *Quantum Optics in Phase Space*; Wiley VCH: Berlin, Germany, 2021.
26. Krantz, P.; Kjaergaard, M.; Yan, F.; Orlando, T.P.; Gustavsson, S.; Oliver, W.D. A Quantum Engineer's Guide to Superconducting Qubits. *Appl. Phys. Rev.* **2019**, *6*, 021318. [CrossRef]
27. Lipkin, H.; Meshkov, N.; Glick, A. Validity of many-body approximation methods for a solvable model. (I). Exact solutions and perturbation theory. *Nucl. Phys.* **1965**, *62*, 188. [CrossRef]
28. Dou, F.-Q.; Wang, Y.-J.; Sun, J.-A. Charging advantages of Lipkin-Meshkov-Glick quantum battery. *arXiv* **2022**, arXiv:2208.04831.
29. Walther, H.; Varcoe, B.T.H.; Englert, B.-G.; Becker, T. Cavity quantum electrodynamics. *Rep. Prog. Phys.* **2006**, *69*, 1325. [CrossRef]
30. Blais, A.; Huang, R.-S.; Wallraff, A.; Girvin, S.M.; Schoelkopf, R. J. Cavity quantum electrodynamics for superconducting electrical circuits: An architecture for quantum computation. *Phys. Rev. A* **2004**, *69*, 062320. [CrossRef]
31. Santos, T.F.; Vianna, Y.; Santos, M.F. Vacuum enhanced charging of a quantum battery. *Phys. Rev. A* **2023**, *107*, 032203. [CrossRef]
32. Roman-Roche, J.; Zueco, D. Effective theory for matter in non-perturbative cavity QED. *SciPost Phys. Lect. Notes* **2022**, *50*, 1–32. [CrossRef]
33. Felicetti, S.; Pedernales, J.S.; Egusquiza, I.L.; Romero, G.; Lamata, L.; Braak, D.; Solano, E. Spectral collapse via two-phonon interactions in trapped ions. *Phys. Rev. A* **2015**, *92*, 033817. [CrossRef]
34. Felicetti, S.; Rossatto, D.Z.; Rico, E.; Solano, E.; Forn-Díaz, P. Two-photon quantum Rabi model with superconducting circuits. *Phys. Rev. A* **2018**, *97*, 013851. [CrossRef]
35. Abah, O.; De Chiara, G.; Paternostro, M.; Puebla, R. Harnessing nonadiabatic excitations promoted by a quantum critical point: Quantum battery and spin squeezing. *Phys. Rev. Res.* **2022**, *4*, L022017. [CrossRef]
36. Larson, J. Interaction-induced Landau-Zener transitions. *Europhys. Lett.* **2010**, *90*, 54001. [CrossRef]
37. Campaioli, F.; Pollock, F.A.; Binder, F.C.; Céleri, L.; Goold, J.; Vinjanampathy, S.; Modi, K. Enhancing the Charging Power of Quantum Batteries. *Phys. Rev. Lett.* **2017**, *118*, 150601. [CrossRef]
38. Le, T.P.; Levinsen, J.; Modi, K.; Parish, M.M.; Pollock, F.A. Spin-chain model of a many-body quantum battery. *Phys. Rev. A* **2018**, *97*, 022106. [CrossRef]
39. Gyhm, J.-Y.; Safránek, D.; Rosa, D. Quantum Charging Advantage Cannot Be Extensive without Global Operations. *Phys. Rev. Lett.* **2022**, *128*, 140501. [CrossRef] [PubMed]
40. Crescente, A.; Ferraro, D.; Carrega, M.; Sassetti, M. Enhancing coherent energy transfer between quantum devices via a mediator. *Phys. Rev. Res.* **2022**, *4*, 033216. [CrossRef]
41. Hu, C.-K.; Qiu, J.; Souza, P.J.P.; Yuan, J.; Zhou, Y.; Zhang, L.; Chu, J.; Pan, X.; Hu, L.; Li, J.; et al. Optimal charging of a superconducting quantum battery. *Quantum Sci. Technol.* **2022**, *7*, 045018. [CrossRef]
42. Rodríguez, C.; Rosa, D.; Olle, J. AI-discovery of a new charging protocol in a micromaser quantum battery. *arXiv* **2023**, arXiv:2301.09408v2
43. Rossini, D.; Andolina, G.M.; Rosa, D.; Carrega, M.; Polini, M. Quantum Advantage in the Charging Process of Sachdev-Ye-Kitaev Batteries. *Phys. Rev. Lett.* **2020**, *125*, 236402. [CrossRef] [PubMed]
44. Allahverdyan, A.E.; Balian, R.; Nieuwenhuizen, T.M. Maximal work extraction from quantum systems. *Europhys. Lett.* **2004**, *67*, 565. [CrossRef]
45. Haroche, S.; Raimond, J.-M. *Exploring the Quantum. Atoms, Cavities and Photons*; Oxford University Press: Oxford, UK, 2006.

46. Devoret, M.H.; Schoelkopf, R.J. Superconducting Circuits for Quantum Information: An Outlook. *Science* **2013**, *339*, 1169. [CrossRef] [PubMed]
47. Wendin, G. Quantum information processing with superconducting circuits: A review. *Rep. Prog. Phys.* **2017**, *80*, 106001 [CrossRef]
48. Julià-Farré, S.; Salamon, T.; Riera, A.; Bera, M.N.; Lewenstein, M. Bounds on the capacity and power of quantum batteries. *Phys. Rev. Res.* **2020**, *2*, 023113. [CrossRef]
49. Fink, J.M.; Bianchetti, R.; Baur, M.; Göppl, M.; Steffen, L.; Filipp, S.; Leek, P. J.; Blais, A.; Wallraff, A. Dressed Collective Qubit States and the Tavis-Cummings Model in Circuit QED. *Phys. Rev. Lett.* **2009**, *103*, 083601. [CrossRef]
50. Giannelli, L.; Rajendran, J.; Macrí, N.; Benenti, G.; Montangero, S.; Paladino, E.; Falci, G. Optimized state transfer in systems of ultrastrongly coupled matter and radiation. *Il Nuovo Cimento* **2022**, *171*, 45–46.
51. Emary, C.; Brandes, T. Chaos and the quantum phase transition in the Dicke model. *Phys. Rev. E* **2003**,*67*, 066203. [CrossRef] [PubMed]
52. Cejnar, P.; Stransky, P.; Macek, M.; Kloc, M. Excited-state quantum phase transitions. *J. Phys. A Math. Theor.* **2021**, *54*, 133001. [CrossRef]
53. Xiang, Z.-L.; Ashhab, S.; You, J.Q.; Nori, F. Hybrid quantum circuits: Superconducting circuits interacting with other quantum systems. *Rev. Mod. Phys.* **2013**, *85*, 623. [CrossRef]
54. Stockklauser, A.; Scarlino, P.; Koski, J. V.; Gasparinetti, S.; Andersen, C.K.; Reichl, C.; Wegscheider, W.; Ihn, T.; Ensslin, K.; Wallraff, A. Strong Coupling Cavity QED with Gate-Defined Double Quantum Dots Enabled by a High Impedance Resonator. *Phys. Rev. X* **2017**, *7*, 011030. [CrossRef]
55. Sakurai, J.J.; Napolitano, J. *Modern Quantum Mechanics*; Cambridge University Press: Cambridge, UK 2021.
56. Andolina, G.M.; Keck, M.; Mari, A.; Giovannetti, V.; Polini, M. Quantum versus classical many-body batteries. *Phys. Rev. B* **2019**, *99*, 205437. [CrossRef]